A tapered beam piezoelectric energy harvester shunted to P-SSHI interface

Hu, Guobiao, Tang, Lihua, Liang, Junrui, Das, Raj

Guobiao Hu, Lihua Tang, Junrui Liang, Raj Das, "A tapered beam piezoelectric energy harvester shunted to P-SSHI interface," Proc. SPIE 11376, Active and Passive Smart Structures and Integrated Systems IX, 1137606 (22 April 2020); doi: 10.1117/12.2554871

SPIE.

Event: SPIE Smart Structures + Nondestructive Evaluation, 2020, Online Only, California, United States

A Tapered Beam Piezoelectric Energy Harvester Shunted to P-SSHI Interface

Guobiao HU[a], Lihua TANG*[a], Junrui LIANG[b], Raj DAS[c]
[a]Department of Mechanical Engineering, University of Auckland, 20 Symonds Street, Auckland 1010, New Zealand;
[b]School of Information Science and Technology, ShanghaiTech University, 393 Middle Huaxia Road, Shanghai 201210, China
[c]School of Engineering, RMIT University, GPO Box 2476, Melbourne, VIC 3001, Australia
* Corresponding author, l.tang@auckland.ac.nz

ABSTRACT

The existing literature shows that using tapered beam can improve the energy harvesting efficiency. Though various methods have been proposed for modelling the piezoelectric energy harvester (PEH) based on a tapered beam, the solutions to the tapered beam energy harvester presented in the existing literature are mathematically cumbersome. Thus, it is difficult to include complicated interface circuits in the modelling and a simple resistive load is often used to represent the energy harvesting circuit. In this paper, a single-degree-of-freedom (SDOF) model is developed for a tapered beam PEH. A corresponding finite element model is built for verification. Subsequently, the tapered beam PEH is shunted to a parallel synchronized switching harvesting on inductor (P-SSHI) interface circuit instead of a simple resistive load. A semi-analytical method is developed for the analysis of the P-SSHI interface circuit with the consideration of the voltage drops in diodes. Using the proposed methods presented in this paper, the mechanical and electrical domains are bridged to provide a comprehensive analysis of a practical tapered beam PEH.

Keywords: tapered beam; single-degree-of-freedom; piezoelectric energy harvesting; P-SSHI

1. INTRODUCTION

Ubiquitous vibration energy has a great potential to be converted into electric energy to power micro-electro-mechanical devices, which has greatly motivated the development of the energy harvesting technology [1-8]. A typical energy harvester is obtained by attaching a piezoelectric patch onto a cantilevered beam [3, 9-12]. When the cantilevered beam vibrates around the resonance, the attached piezoelectric patch delivers a maximum power output. To model such kind of typical energy harvesters, various methods including analytical distributed parameter model [3], simplified SDOF model [9, 10], equivalent circuit model [11], spectral element model [13] and finite element model [14, 15] have been proposed.

Broadening the operation bandwidth and increasing the power output are the two main problems that have been extensively studied. To broaden the bandwidth, solutions that can be found in the existing literature include using the multi-modal technique [16-18], introducing nonlinearities [19-21], employing self-tuning structures [22, 23]. More information on the these broadband techniques can be found in [24, 25]. For the second problem, methods for enhancing power output include the optimization of the mechanical structure and the interface circuits.

Regarding mechanical structural optimization, Roundy *et al.* [26] proposed to use a beam with variable cross section to improve the power output. Mehraeen *et al.* [27] experimentally proved that a tapered beam can increase the power as compared to a rectangular beam. Matova *et al.* [28] investigated the effect of the length/width ratio on the performance of a tapered beam PEH. In recent, Wang *et al.* [29] introduced the tapered beam structure for galloping energy harvesting. The results showed that using the tapered beam can increase the power for about 61%. Regarding the modelling of the tapered beam PEH, Goldschmidtboeing *et al.* [30] developed a modelling method based the Rayleigh–Ritz method. Dietl *et al.* [31] developed the analytical model of a beam with non-uniform width. Salmani *et al.* [32] derived a finite element model based on which they optimized the tapered beam PEH to achieve the most effective tapering profile. According to the state-of-the-art, there lacks a lumped parameter modelling method for the tapered beam PEH as that for the typical rectangular beam PEH [9]. Due to that the existing modelling methods are complicated, only a simple resistive interface

Active and Passive Smart Structures and Integrated Systems IX, edited by Jae-Hung Han, Gang Wang, Shima Shahab,
Proc. of SPIE Vol. 11376, 1137606 · © 2020 SPIE · CCC code: 0277-786X/20/$21 · doi: 10.1117/12.2554871

circuit can be considered. Therefore, to simplify the modelling of a tapered beam PEH, one motivation of this paper is to develop a SDOF model of the tapered beam PEH to fill this gap.

On the other hand, using advanced interface circuits, such as synchronized charge extraction (SCE) [33, 34], synchronized switch harvesting on inductor (SSHI) [35-37], can also boost the power output from the energy harvesters. A study showed that a highly efficient P-SSHI interface circuit can increase the power output for about 5.8 times [38]. However, due to the complicated architectures of the advanced interface circuits, the corresponding circuit analysis becomes difficult. Though Yang *et al.* [11] presented an equivalent circuit model (ECM) of a tapered beam PEH that enabled the consideration of complicated interface circuit, the ECM method is intrinsically a numerical method and strongly relies on commercial circuit simulation software. Available approaches for the analysis of the P-SSHI interface circuit include an analytical method [36] and an equivalent impedance method [37]. However, the limitation of the analytical method presented in [36] is that the electrical components are under the ideal assumption, thus the analytical method often overestimates the power output from the P-SSHI circuit. The equivalent impedance method does not need to assume the diodes to be ideal and can take the voltage drops into account to further improve the prediction accuracy. However, the weakness of the equivalent impedance method is that an unknown parameter is required to be determined from the experiment. To overcome these issues, a semi-analytical method is developed for the analysis of a P-SSHI interface circuit with non-zero voltage drops in diodes.

The rest of the paper is organized as follows: In section 2, a SDOF model of the tapered beam is developed and the explicit expressions of the equivalent parameters are derived. A corresponding finite element model is also built for verification. In section 3, a semi-analytical method for the analysis of the P-SSHI interface circuit is developed. For an example of a tapered beam shunted to a P-SSHI interface circuit, the results from the semi-analytical method are compared with the analytical method presented in [36]. In the last section 4, conclusions of the work presented in this paper are summarized.

2. SDOF MODEL OF TAPERED BEAM PEH

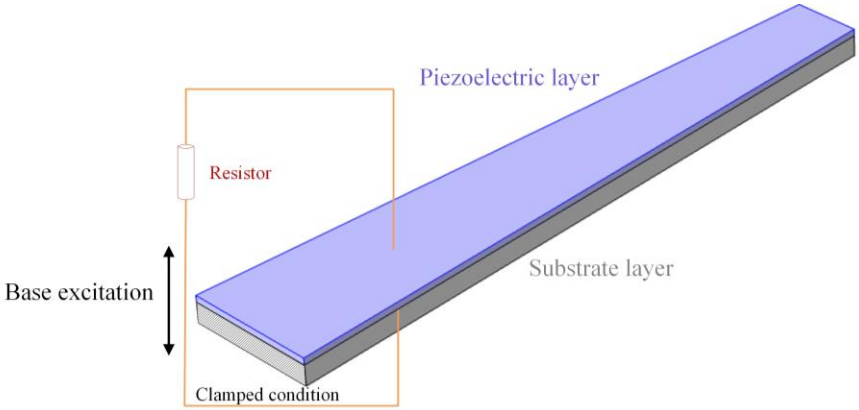

Figure 1. Schematic of the tapered beam PEH.

For a linearly tapered beam as shown in Figure 1, the bending stiffness $EI(x)$ and the mass per unit length $m(x)$ are linearly varied along the length direction and can be formulated as follows

$$m(x) = m_0(ax+1) \tag{1}$$

$$EI(x) = EI_0(ax+1) \tag{2}$$

Under the gravity which is perpendicular to the beam, the shear force in the tapered beam at an arbitrary position x can be derived as

$$F(x) = -\frac{1}{2}m_0 gax^2 - m_0 gx + \frac{1}{2}m_0 gaL^2 + m_0 gL + M_t g \tag{3}$$

where g is the gravitational constant. L is the length of the tapered beam. M_t is the tip mass attached at the tip of the beam. However, it should be mentioned that we only consider a tapered beam without tip mass in this paper. M_t is introduced only as an intermediate parameter to assist the following derivation. The bending moment in the beam is:

$$M(x)=\frac{1}{6}m_0gax^3+\frac{1}{2}m_0gx^2-\left(\frac{1}{2}m_0gaL^2+m_0gL+M_tg\right)x+\frac{1}{3}m_0gaL^3+\frac{1}{2}m_0gL^2+M_tgL \tag{4}$$

Using the relationship between the bending moment and the deflection from the beam theory, the static deflection under gravity of the tapered beam is derived

$$y(x)=\int_0^x\int_0^x\frac{M(x)}{EI(x)}dxdx \tag{5}$$

Note that the quadratic integral introduces two unknown constants, the clamped boundary condition implies the displacement and the slope of the clamped end are zeroes

$$\begin{cases}y(0)=0\\ y'(0)=0\end{cases} \tag{6}$$

Using Eq.(6), the two unknown integral constants in Eq.(5) can be determined. To represent the tapered beam as a SDOF system, we assume that the lumped parameters are concentrated at the tip of the tapered beam. First, consider the situation when $M_t=0$, the deflection of the tip of the tapered beam is

$$\frac{M_{static}g}{K}=y(L,M_t=0) \tag{7}$$

When $M_t\neq 0$, the deflection of the tip of the tapered beam becomes

$$\frac{(M_{static}+M_t)g}{K}=y(L,M_t\neq 0) \tag{8}$$

Since the equivalent stiffness of the beam (i.e., K) is assumed to be constant, combining Eqs.(7) and (8), K can be derived

$$K=\frac{M_tg}{y(L,M_t\neq 0)-y(L,M_t=0)}=\frac{3a^3EI_0}{2a^2L^2\psi+4L\psi+2\psi-3a^2L^2-2aL} \tag{9}$$

where $\psi=\ln(aL+1)$. Neglecting the tip mass, using the Rayleigh's method can derive the approximate fundamental natural frequency of the tapered beam. The derived static deflection function $y(x)$ can be used as the assumed fundamental mode shape. The maximum potential energy P in the beam is:

$$P=\frac{1}{2}\int_0^L EI(x)\left(\frac{d^2y(x)}{dx^2}\right)^2dx \tag{10}$$

The maximum kinetic energy T in the beam is

$$T=\frac{1}{2}\omega_n^2\int_0^L m(x)y^2(x)dx \tag{11}$$

Equating P (i.e., Eq.(10)) and T (i.e., Eq.(11)) yields the solution to ω_n which is the fundamental natural frequency of the tapered beam. Consequently, the equivalent dynamic mass of the tapered beam is derived

$$M=\frac{K}{\omega_n^2}=\frac{m_0\sum_{p=0}^{10}n_p(aL)^p}{7350a\left[\sum_{q=0}^{6}d_q(aL)^q\right]\left[\sum_{r=0}^{2}h_r(aL)^r\right]} \tag{12}$$

where

$$\begin{cases} n_{10}=88200\psi^2-322140\psi+295913 \\ n_9=882000\psi^2-2721600\psi+2034920 \\ n_8=3969000\psi^2-10174500\psi+6056595 \\ n_7=10584000\psi^2-22104600\psi+10229690 \\ n_6=18522000\psi^2-30781800\psi+10769395 \\ n_5=22226400\psi^2-28523880\psi+7262598 \\ n_4=18522000\psi^2-17610600\psi 3070515 \\ n_3=10584000\psi^2-6993000\psi 742980 \\ n_2=3969000\psi^2-1619100\psi+76230 \\ n_1=882000\psi^2-163800\psi-1260 \\ n_0=88200\psi^2+1260\psi \end{cases};\quad \begin{cases} d_6=24\psi-45 \\ d_5=144\psi-198 \\ d_4=360\psi-342 \\ d_3=480\psi-296 \\ d_2=360\psi-132 \\ d_1=144\psi-24 \\ d_0=24\psi \end{cases};\quad \begin{cases} h_2=2\psi-3 \\ h_1=4\psi-2 \\ h_0=2\psi \end{cases}$$

The tapered beam is covered by a layer of piezoelectric material for converting vibration energy into electrical energy. The electromechanical coupling coefficient can be determined using the following equation [9]

$$\Theta=-e_{31}h_{pc}\frac{\int_0^L b(x)\frac{d^2\beta_1(x)}{dx^2}dx}{\beta_1(L)} \tag{13}$$

where e_{31} is the piezoelectric constant, h_{pc} is the distance between the center of the piezoelectric transducer in the thickness direction to the neutral axis [9, 10], $\beta_1(x)$ is the fundamental mode shape of the tapered beam. The analytical solution to $\beta_1(x)$ is cumbersome. The derived static deflection function $y(x)$ can be used to approximate the exact fundamental mode shape. The explicit expression of the electromechanical coupling coefficient (i.e., Θ) can be obtained

$$\Theta=-\frac{3e_{31}h_{pc}b_0a^4L^2\left(3m_0aL^2+4m_0L\right)}{\left(\begin{array}{l}24m_0\psi a^4L^4-41m_0a^4L^4+96m_0\psi a^3L^3-104m_0a^3L^3\\+144m_0\psi a^2L^2-84m_0a^2L^2+96m_0\psi aL-24m_0aL+24m_0\psi\end{array}\right)} \tag{14}$$

where $b_0=b(0)$ is the width of the tapered beam at the root. Hence, the tapered beam with piezoelectric coverage can be equivalently represented by a SDOF model and the governing equations can be expressed as

$$\begin{cases} M\ddot{u}+D\dot{u}+Ku+\Theta v=-M\ddot{u}_b \\ \dfrac{v}{R}+C_p\dot{v}-\Theta\dot{u}=0 \end{cases} \tag{15}$$

where v is the voltage across the piezoelectric transducer. R is the electric resistor connected to the piezoelectric transducer. $C_p=\varepsilon_{33}^S\left(b(0)+b(L)\right)L/2h_p$ is the capacitance of the piezoelectric transducer, in which ε_{33}^S is the permittivity at constant stress, h_p is the thickness of the piezoelectric transducer, $b(L)$ is the width of the tapered beam at the tip, respectively. $D=2\zeta M\omega_n$ is the damping coefficient. ζ is the damping ratio. u_b is the base displacement. The

displacement at the tip of the tapered beam is redefined as u for conciseness. For the SDOF representation of a cantilevered beam, it has been pointed out that a factor is required to correct the forcing term in the electromechanically coupled governing equations [10]. The analytical expression of the correction factor should be

$$\mu = \beta_1(L) \int_{x=0}^{L} m(x)\beta_1(x)dx \tag{16}$$

Using the derived static deflection function to approximate the exact fundamental mode shape, the correction factor can be calculated as

$$\mu = \frac{y(L) \int_{x=0}^{L} m(x)y(x)dx}{\int_{x=0}^{L} m(x)y^2(x)dx} \tag{17}$$

The explicit expression of μ is complicated, one can use a symbolic computing software such as Maple or Mathematica to calculate Eq.(17). After obtaining the correction factor, the governing equations (i.e., Eq.(15)) of the electromechanical system become:

$$\begin{cases} M\ddot{u} + D\dot{u} + Ku + \Theta v = -\mu M\ddot{u}_b \\ \dfrac{v}{R} + C_p\dot{v} - \Theta\dot{u} = 0 \end{cases} \tag{18}$$

Table 1. Geometric and material parameters of the tapered beam PEH under investigation.

Parameters	Values	Materials	Parameters	Values
Substrate beam length L	100 mm	Aluminum	Mass density	2700 kg/m^3
Substrate beam root width $b(0)$	20 mm		Young's Modulus	69.5 GPa
Substrate beam tip width $b(L)$	varying	Piezoelectric material	Mass density	5440 kg/m^3
Substrate beam thickness	0.6 mm		Young's Modulus	30.336 GPa
Piezoelectric layer thickness	0.2 mm		Piezoelectric constant e_{31}	-5.187 C/m^2
Resistance	varying		Permittivity at constant stress ε_{33}^S	1.3281×10-8 F/m

To verify the developed SDOF model, a corresponding finite element mode is built using the commercial software ANSYS. For the given system parameters listed in Table 1 and $b(L)$ = 10mm, Figure 2 shows the voltage response of the tapered beam PEH calculated using the developed SDOF model and ANSYS. The detailed procedure of calculating the bending stiffness and the mass per unit length of the two-layered tapered beam using the parameters listed in Table 1 can be referred to [9]. The resistance is fixed at 400 kΩ and an acceleration field with amplitude A_{cc} = 10m/s^2 is applied onto the whole structure to ensure a constant input power level over the spectrum under investigation. It is worth mentioning that there is a minor difference between the natural frequencies calculated using the developed SDOF model and ANSYS. To focus on the comparison of the output voltage amplitude, the frequency axes for the developed SDOF model and ANSYS are normalized by each natural frequency, separately. It can be seen that both results from the developed SDOF model and ANSYS match well with each other. By varying the tip width of the tapered beam, Table 2 lists a few more comparison examples in details. It can be found that in term of the natural frequency in short circuit condition (R = 0Ω), the prediction error of the developed SDOF model is smaller than 1%. Regarding the maximum voltage amplitude, the prediction error of the developed SDOF model is smaller than 5%.

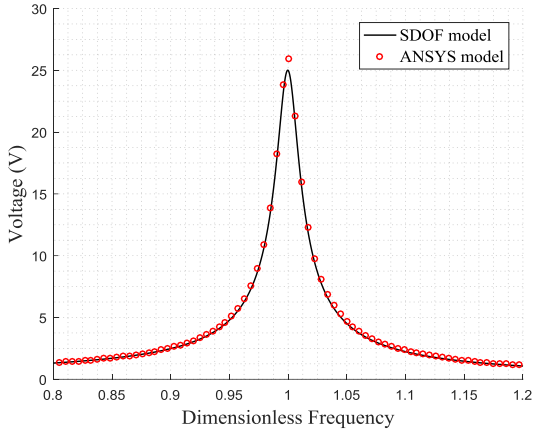

Figure 2. Voltage response of the tapered PEH with the tip width $b(L)$ of 10 mm.

Table 2. The short-circuit natural frequencies and the maximum voltage amplitudes of the tapered beam PEH with different tip widths calculated using the SDOF model and ANSYS.

Tip width - $b(L)$	**Short-circuit natural frequency**		**Maximum voltage amplitude**	
	SDOF model	ANSYS	SDOF model	ANSYS
12 mm	58.00 Hz	57.69 Hz	26.3 V	27.4 V
10 mm	61.13 Hz	60.76 Hz	25.0 V	26.0 V
8 mm	65.02 Hz	64.56 Hz	23.5 V	24.5 V
6 mm	70.00 Hz	69.44 Hz	21.8 V	22.8 V
4 mm	76.73 Hz	76.00 Hz	19.8 V	20.8 V

3. P-SSHI INTERFACE CIRCUIT ANALYSIS

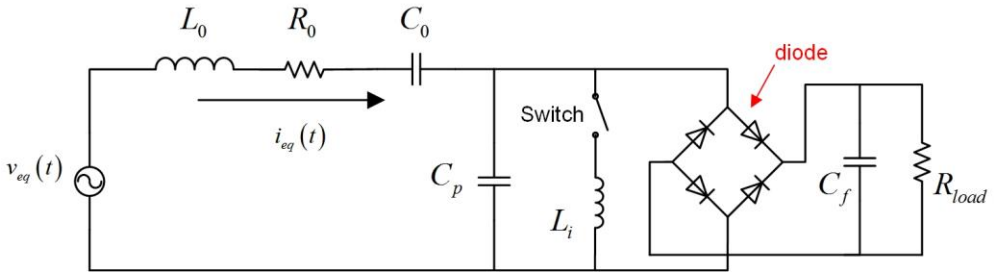

Figure 3. Equivalent circuit representation of a SDOF tapered beam PEH shunted to a P-SSHI interface circuit.

In this section, the tapered beam PEH is shunted to a P-SSHI interface circuit. A semi-analytical method is developed for addressing the circuit analysis in consideration of the voltage drops in the diodes of the P-SSHI interface circuit. Based on the mechanical-electrical analogies, the mechanical SDOF model derived in section 2 can be equivalently represented by an electrical model [9]. The equivalent circuit parameters of the mechanical parameters are

$$L_0 = M/\Theta^2 \quad C_0 = \Theta^2/K \quad R_0 = D/\Theta^2 \quad v_{eq}(t) = -\mu M\ddot{u}_b/\Theta \quad i_{eq}(t) = \Theta\dot{u} \tag{19}$$

The mechanical system and the electric circuit part are thus coupled as shown in Figure 3.

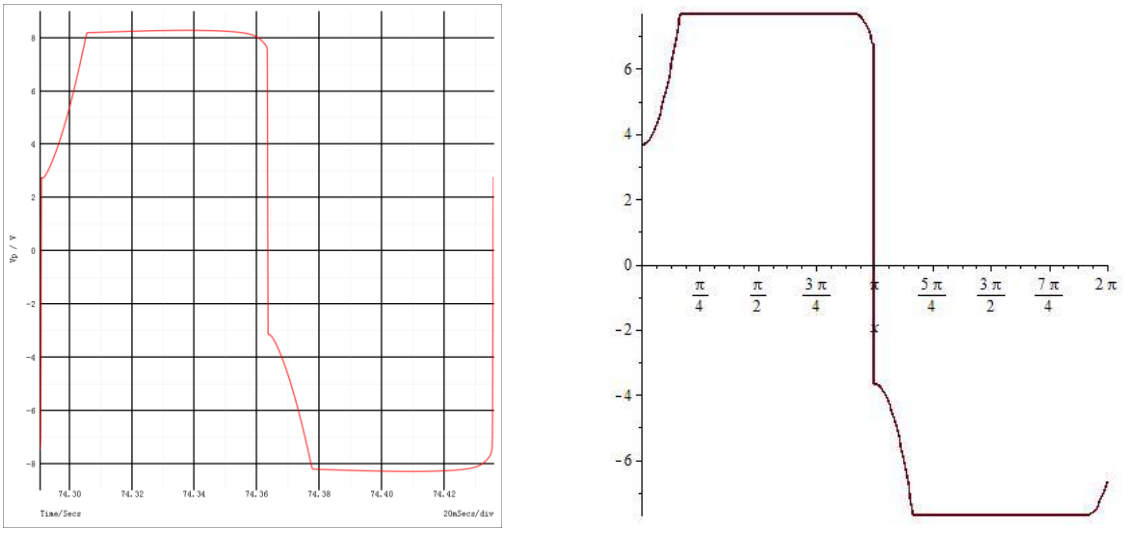

(a) (b)

Figure 4. Voltage waveforms in one cycle from (a) simulation; (b) the piecewise function.

Figure 4(a) shows the waveform of the voltage across the piezoelectric element in P-SSHI. According to the characteristics of the waveform, the voltage across the piezoelectric element is depicted by the following piecewise function (as shown in Figure 4(b))

$$v_p(t)=\begin{cases} V_{oc}\left[1-\cos(\omega t)\right]+\gamma\left[V_{oc}\left(1-\cos\phi\right)-V_{rect}\right] & 0\le\omega t<\theta \\ V_{rect} & \theta\le\omega t\le\pi-\phi \\ V_{rect}-V_{oc}\left[1+\cos\left(\omega t+\phi\right)\right] & \pi-\phi\le\omega t\le\pi \\ \gamma\left[V_{rect}-V_{oc}\left(1-\cos\phi\right)\right]-V_{oc}\left[1+\cos(\omega t)\right] & \pi\le\omega t<\pi+\theta \\ -V_{rect} & \pi+\theta\le\omega t<2\pi-\phi \\ V_{oc}\left[1-\cos\left(\omega t+\phi\right)\right]-V_{rect} & 2\pi-\phi\le\omega t\le 2\pi \end{cases} \tag{20}$$

where γ is the voltage inversion factor in every switching action. θ corresponds to the rectifier blocked angle in a half cycle. V_{rect} is the rectified voltage across the piezoelectric element and the rectified voltage across the resistor should be $V_{rect}^{*}=V_{rect}-2V_D$. V_{oc} is the magnitude of the open circuit voltage. ϕ is the phase lag between the instants of switching action start and the maximum (or minimum) $v_p(t)$

$$\cos\phi=1-\frac{V_D}{V_{oc}} \tag{21}$$

$$\phi=\cos^{-1}\left(1-\frac{V_D}{V_{oc}}\right) \tag{22}$$

where V_D is the forward voltage drop in the diode. By defining the non-dimensional parameter $\tilde{V}_D=\frac{V_D}{V_{oc}}$, we have

$$\cos\phi=1-\tilde{V}_D \tag{23}$$

$$\tilde{V}_D=1-\cos\phi \tag{24}$$

V_{oc} can be expressed as

$$V_{oc} = \frac{I_0}{\omega C_p} = \frac{\Theta U}{C_p} \tag{25}$$

where I_0 is the magnitude of the equivalent current $i_{eq}(t)$, U is the magnitude of the relative displacement u. One obtains the relationship between V_{rect} and V_{oc}

$$V_{oc}(1-\cos\theta) + \gamma\left[V_{oc}(1-\cos\phi) - V_{rect}\right] = V_{rect} \tag{26}$$

Therefore, V_{rect} can be expressed in terms of V_{oc}

$$V_{rect} = \frac{(1-\cos\theta) + \gamma(1-\cos\phi)}{(1+\gamma)} V_{oc} \tag{27}$$

θ can be expressed as

$$\cos\theta = 1 + \gamma(1-\cos\phi) - (1+\gamma)\tilde{V}_{rect} \tag{28}$$

where $\tilde{V}_{rect} = \frac{V_{rect}}{V_{oc}}$. The fundamental harmonic component of $v_p(t)$ can be calculated:

$$v_{p,F} = \frac{V_{oc}}{\pi}\left\{\begin{array}{l} -\left[\begin{array}{l}\left(2(\cos\phi+\alpha-1)\gamma - 2 + 2\alpha + \cos\theta\right)\sin\theta \\ +\phi\cos\phi - \sin\phi + \theta\end{array}\right]\cos(\omega t) \\ +\left[\begin{array}{l}\left(2(\cos\phi-1+\alpha)\gamma + \cos\theta + 2\alpha - 2\right)\cos\theta \\ +\phi\sin\phi + 2(1-\gamma)\cos\phi + 2(1-\alpha)\gamma + 2\alpha - 1\end{array}\right]\sin(\omega t)\end{array}\right\} \tag{29}$$

where $\alpha = \tilde{V}_{rect}$. Combining Eq.(25) and Eq.(29) and using Fourier transform, the equivalent impedance of the electrical part can be derived as:

$$Z_{elec} = \frac{1}{\pi\omega C_p}\left\{\begin{array}{l}\left[\begin{array}{l}\left(2(\cos\phi-1+\alpha)\gamma + \cos\theta + 2\alpha - 2\right)\cos\theta \\ +\phi\sin\phi + 2(1-\gamma)\cos\phi + 2(1-\alpha)\gamma + 2\alpha - 1\end{array}\right] \\ -j\left[\begin{array}{l}\left(2(\cos\phi+\alpha-1)\gamma - 2 + 2\alpha + \cos\theta\right)\sin\theta \\ +\phi\cos\phi - \sin\phi + \theta\end{array}\right]\end{array}\right\} \tag{30}$$

Considering the charge balance during one period

$$\int_{t_i^+}^{t_f}\left\{-\Theta\dot{u}(t) + C_p\dot{v}_p(t)\right\}dt = -2\Theta U + C_p V_{rect}(1+\gamma) = -\frac{T}{2}\frac{(V_{rect} - 2V_D)}{R_{load}} \tag{31}$$

We have

$$V_{rect} = \frac{2\omega R_{load}\Theta U + 2\pi V_D}{\left[\omega R_{load} C_p(1+\gamma) + \pi\right]} \tag{32}$$

Recalling that $V_{oc} = \frac{\Theta}{C_p}U$, we have

$$\alpha = \frac{2\omega R_{load} C_p + 2\pi(1-\cos\phi)}{\left[\omega R_{load} C_p(1+\gamma) + \pi\right]} \tag{33}$$

Substituting Eq.(33) into Eq.(28) yields

$$\cos\theta = 1+\gamma(1-\cos\phi)-(1+\gamma)\alpha \tag{34}$$

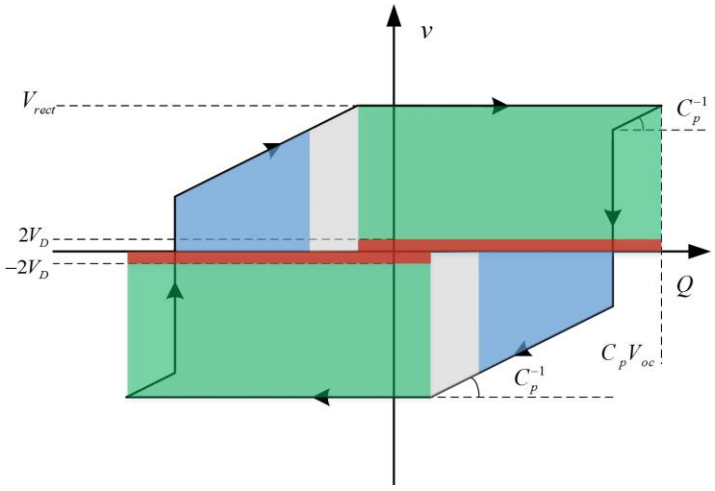

Figure 5. The charge-voltage diagram.

Figure 5 shows the charge–voltage locus of the capacitance C_p of the piezoelectric transducer and reveals the energy flow in the system [39]. The areas marked in green, blue, red and grey represent the harvested energy, the energy dissipated in the switching path, the energy dissipated by the bridge rectifier and the energy returns from the electrical circuit to the mechanical part, respectively. Based on the geometric relationship as shown in Figure 5, the amount of energy harvested in one cycle can be calculated as

$$E_h = 2C_pV_{oc}^2\left(\tilde{V}_{rect}-2\tilde{V}_D\right)\left[2-(1+\gamma)\tilde{V}_{rect}-(1-\gamma)(1-\cos\phi)\right] \tag{35}$$

Thus, the harvested power is

$$P_h = E_h\frac{\omega}{2\pi} \tag{36}$$

Using Joule's law and noting that I_0 denotes the amplitude of the AC current, the equivalent resistance that corresponds to the harvesting component can be derived as

$$R_h = \frac{2P_h}{I_0^2} = \frac{2P_h}{\omega^2C_p^2V_{oc}^2} = \frac{2}{\pi\omega C_p}\left[\alpha-2(1-\cos\phi)\right]\left[2-(1+\gamma)\alpha-(1-\gamma)(1-\cos\phi)\right] \tag{37}$$

By dividing the equivalent electrical impedance (i.e, Eq.(30)) into real and imaginary parts, in conjunction with Eq.(37), we can derive the equivalent dissipative components and the inductance of the P-SSHI electrical part as

$$\begin{cases} R_E = \dfrac{1}{\pi\omega C_p}\left[\begin{array}{l}\left(2(\cos\phi-1+\alpha)\gamma+\cos\theta+2\alpha-2\right)\cos\theta \\ +\phi\sin\phi+2(1-\gamma)\cos\phi+2(1-\alpha)\gamma+2\alpha-1\end{array}\right] \\ R_h = \dfrac{2}{\pi\omega C_p}\left[\alpha-2(1-\cos\phi)\right]\left[2-(1+\gamma)\alpha-(1-\gamma)(1-\cos\phi)\right] \\ R_d = R_E - R_h \\ X_E = -\dfrac{1}{\pi\omega C_p}\left[\begin{array}{l}\left(2(\cos\phi+\alpha-1)\gamma-2+2\alpha+\cos\theta\right)\sin\theta \\ +\phi\cos\phi-\sin\phi+\theta\end{array}\right] \end{cases} \tag{38}$$

Using impedance-based analysis, we can derive the expressions of the harvested power P_h and the rectified voltage V_{rect}^*

$$P_h = \frac{V_{eq}^2}{2} \frac{R_h}{\left(X_{L_0} + X_{C_0} + X_E\right)^2 + \left(R_E + R_0\right)^2} \tag{39}$$

$$V_{rect}^* = \sqrt{P_h R_{load}} \tag{40}$$

where V_{eq} is the magnitude of the equivalent voltage $v_{eq}(t)$. It is worth noting that Eqs.(39) and (40) can not be directly solved, because of the introduction of an additional unknown parameter ϕ. To numerically address this problem, a semi-analytical scheme as illustrated in Figure 6 is proposed to explore the suitable solution. The key of the proposed solution scheme is assuming a ϕ first to remove the unknown parameter and complete the calculation, and then comparing the calculated ϕ with the assumed ϕ. If the calculated ϕ matches the assumed ϕ, the solution scheme is finished and the solution is obtained. Otherwise, one needs to restart another round of calculation until the satisfactory ϕ is found.

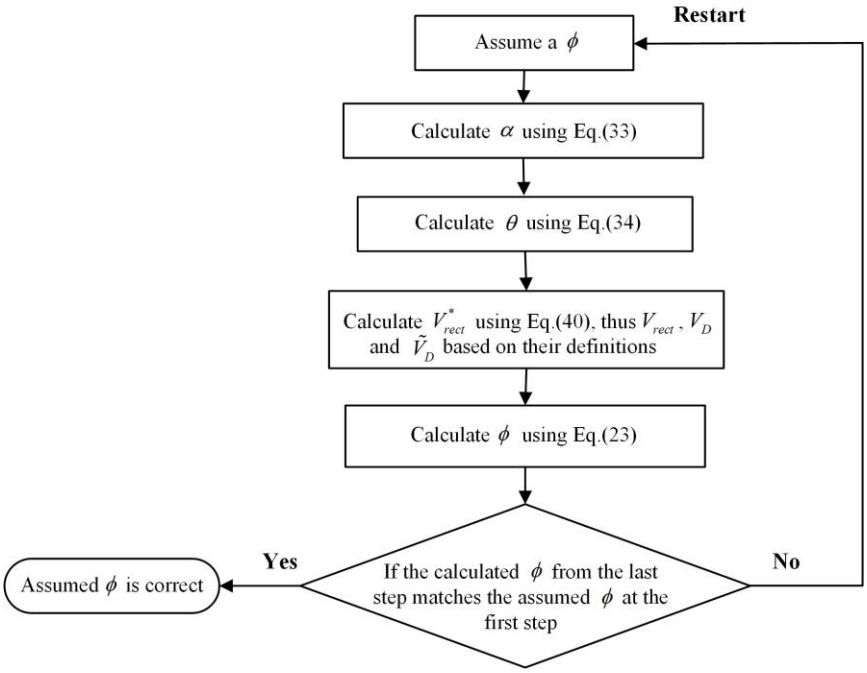

Figure 6. Solution scheme.

Using the developed semi-analytical method, the energy harvesting performance of the tapered beam PEH shunted to the P-SSHI interface circuit is evaluated. The results from the analytical method presented in [36] are also provided for comparison. First, we assume that the didoes are ideal, i.e., $V_D = 0\text{V}$. Figure 7(a) and (b) show the voltage and power output responses from the P-SSHI interface circuit. It can be found that the developed semi-analytical method matches the analytical method very well. Subsequently, the voltage drops are introduced. By setting $V_D = 0.2\text{V}$, Figure 7(c) and (d) show the corresponding results. It can be seen that the maximum voltage amplitude from the analytical method under the assumption of ideal didoes is about 20.33V, while the result from the developed semi-analytical method is about 19.14V. It can be found that the semi-analytical method successfully predicts the voltage reduction due to the existence of the voltage drops in the diodes. From Figure 7(d), the maximum power outputs predicted by the analytical and the developed semi-analytical methods are 1.033mW and 0.916mW, respectively. Due to the existence of the minor voltage drops V_D in the diodes, the power output is reduced for about 11.3%.

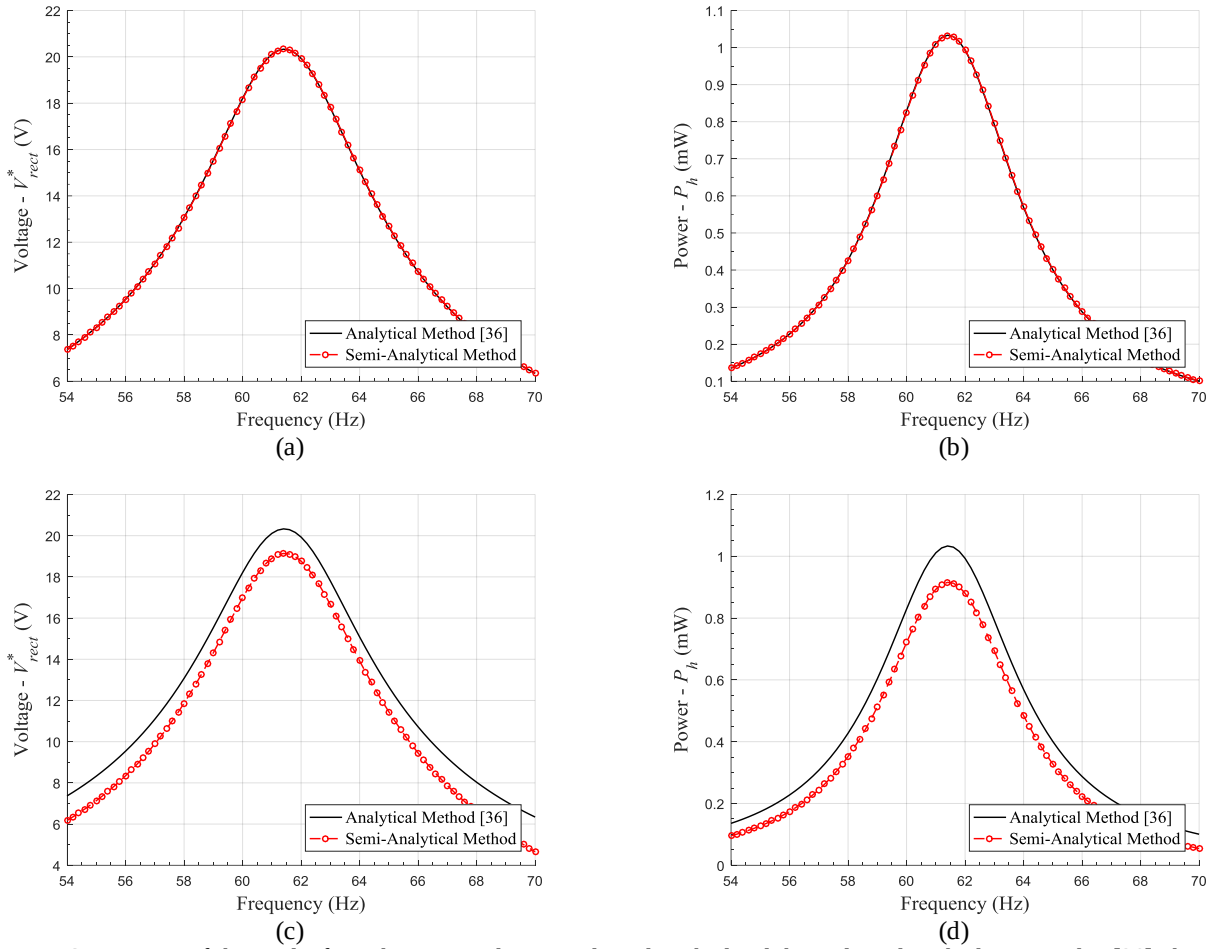

Figure 7. Comparison of the results from the proposed semi-analytical method and the analytical method presented in [36]: the voltage response (a) $V_D = 0\text{V}$, (c) $V_D = 0.2\text{V}$; the power response (b) $V_D = 0\text{V}$, (d) $V_D = 0.2\text{V}$. The resistance is fixed at $R_{load} = 400\ \text{k}\Omega$.

4. CONCLUSIONS

This paper has presented a comprehensive study of a tapered beam PEH that is shunted to a P-SSHI interface circuit. To simplify the modelling of the mechanical structure, a SDOF representation method is developed. Explicit expressions of the equivalent parameters have been derived based on the approximation of the fundamental mode shape by the static deflection. A finite element has been built for the verification of the developed SDOF model. The result showed that the prediction error of the developed SDOF model was less than 1% in terms of the natural frequency and 5% in terms of the maximum voltage amplitude. To improve the circuit analysis, a semi-analytical method has been developed for the analysis of the P-SSHI interface circuit by taking the voltage drops of diodes into account. For a given example, the results from the developed semi-analytical method matched well with those from the analytical method in the existing literature when the voltage drops were ignored. For the existence of the voltage drops, the developed semi-analytical method successfully predicted the the voltage and power reduction compared to the ideal diode scenario.

REFERENCES

[1]. Priya, S. and D.J. Inman, Energy harvesting technologies. Vol. 21. 2009, New York: Springer.
[2]. Tang, L., Y. Yang, and C.K. Soh, Broadband Vibration Energy Harvesting Techniques, in Advances in Energy Harvesting Methods, N. Elvin and A. Erturk, Editors. 2013, Springer New York: New York, NY. p. 17-61.

[3]. Erturk, A. and D.J. Inman, A distributed parameter electromechanical model for cantilevered piezoelectric energy harvesters. Journal of Vibration and Acoustics-Transactions of the Asme, 2008. 130(4): p. 041002.
[4]. Fang, S., X. Fu, X. Du, and W.-H. Liao, A music-box-like extended rotational plucking energy harvester with multiple piezoelectric cantilevers. Applied Physics Letters, 2019. 114(23): p. 233902.
[5]. Wang, J., L. Tang, L. Zhao, G. Hu, R. Song, and K. Xu, Equivalent circuit representation of a vortex - induced vibration - based energy harvester using a semi - empirical lumped parameter approach. International Journal of Energy Research, 2020.
[6]. Zhang, M., G. Hu, and J. Wang, Bluff body with built - in piezoelectric cantilever for flow - induced energy harvesting. International Journal of Energy Research, 2020.
[7]. Chen, Z., B. Guo, Y. Yang, and C. Cheng, Metamaterials-based enhanced energy harvesting: A review. Physica B: Condensed Matter, 2014. 438: p. 1-8.
[8]. Fang, S., S. Wang, S. Zhou, Z. Yang, and W.-H. Liao, Exploiting the advantages of the centrifugal softening effect in rotational impact energy harvesting. Applied Physics Letters, 2020. 116(6): p. 063903.
[9]. Hu, G., L. Tang, J. Liang, and R. Das, Modelling of a cantilevered energy harvester with partial piezoelectric coverage and shunted to practical interface circuits. Journal of Intelligent Material Systems and Structures, 2019. 30(13): p. 1045389X19849269.
[10]. Erturk, A. and D.J. Inman. Mechanical considerations for modeling of vibration-based energy harvesters. in Proceedings of the ASME IDETC 21st Biennial Conference on Mechanical Vibration and Noise. 2007.
[11]. Yang, Y. and L. Tang, Equivalent circuit modeling of piezoelectric energy harvesters. Journal of Intelligent Material Systems and Structures, 2009. 20(18): p. 2223-2235.
[12]. Hu, G., B. Zhao, L. Tang, J. Liang, and R. Das. Modeling of partially covered piezoelectric energy harvester connected to SEH interface circuit. 2018. KATHOLIEKE UNIV LEUVEN, DEPT WERKTUIGKUNDE.
[13]. Wang, G., Analysis of bimorph piezoelectric beam energy harvesters using Timoshenko and Euler–Bernoulli beam theory. Journal of Intelligent Material Systems and Structures, 2013. 24(2): p. 226-239.
[14]. Hu, G., L. Tang, and R. Das, General Framework for Modeling Multifunctional Metamaterial Beam Based on a Derived One-Dimensional Piezoelectric Composite Finite Element. Journal of Aerospace Engineering, 2018. 31(6): p. 04018088.
[15]. Abdelkefi, A., N. Barsallo, L. Tang, Y. Yang, and M.R. Hajj, Modeling, validation, and performance of low-frequency piezoelectric energy harvesters. Journal of Intelligent Material Systems and Structures, 2014. 25(12): p. 1429-1444.
[16]. Tang, L.H. and Y.W. Yang, A multiple-degree-of-freedom piezoelectric energy harvesting model. Journal of Intelligent Material Systems and Structures, 2012. 23(14): p. 1631-1647.
[17]. Wu, H., L. Tang, Y. Yang, and C.K. Soh, A novel two-degrees-of-freedom piezoelectric energy harvester. Journal of Intelligent Material Systems and Structures, 2013. 24(3): p. 357-368.
[18]. Kim, I.-H., H.-J. Jung, B.M. Lee, and S.-J. Jang, Broadband energy-harvesting using a two degree-of-freedom vibrating body. Applied Physics Letters, 2011. 98(21): p. 214102.
[19]. Hu, G., L. Tang, R. Das, and P. Marzocca, A two-degree-of-freedom piezoelectric energy harvester with stoppers for achieving enhanced performance. International Journal of Mechanical Sciences, 2018. 149: p. 500-507.
[20]. Xu, J. and J. Tang, Multi-directional energy harvesting by piezoelectric cantilever-pendulum with internal resonance. Applied Physics Letters, 2015. 107(21): p. 213902.
[21]. Wu, Y., J. Qiu, F. Kojima, H. Ji, W. Xie, and S. Zhou, Design methodology of a frequency up-converting energy harvester based on dual-cantilever and pendulum structures. AIP Advances, 2019. 9(4): p. 045312.
[22]. Jo, S., M. Kim, and Y. Kim. Passive-self-tunable vibrational energy harvester. in Solid-State Sensors, Actuators and Microsystems Conference (TRANSDUCERS), 2011 16th International. 2011. IEEE.
[23]. Yu, L., L. Tang, and T. Yang, Experimental investigation of a passive self-tuning resonator based on a beam-slider structure. Acta Mechanica Sinica, 2019. 35(5): p. 1079-1092.
[24]. Tang, L., Y. Yang, and C.K. Soh, Toward broadband vibration-based energy harvesting. Journal of intelligent material systems and structures, 2010. 21(18): p. 1867-1897.
[25]. Twiefel, J. and H. Westermann, Survey on broadband techniques for vibration energy harvesting. Journal of Intelligent Material Systems and Structures, 2013. 24(11): p. 1291-1302.
[26]. Roundy, S., E.S. Leland, J. Baker, E. Carleton, E. Reilly, E. Lai, B. Otis, J.M. Rabaey, P.K. Wright, and V. Sundararajan, Improving power output for vibration-based energy scavengers. IEEE Pervasive computing, 2005. 4(1): p. 28-36.

[27]. Mehraeen, S., S. Jagannathan, and K.A. Corzine, Energy harvesting from vibration with alternate scavenging circuitry and tapered cantilever beam. IEEE Transactions on Industrial Electronics, 2009. 57(3): p. 820-830.
[28]. Matova, S., M. Renaud, M. Jambunathan, M. Goedbloed, and R. Van Schaijk, Effect of length/width ratio of tapered beams on the performance of piezoelectric energy harvesters. Smart Materials and Structures, 2013. 22(7): p. 075015.
[29]. Wang, L., T. Tan, Z. Yan, and Z. Yan, Tapered galloping energy harvester for power enhancement and vibration reduction. Journal of Intelligent Material Systems and Structures, 2019. 30(18-19): p. 2853-2869.
[30]. Goldschmidtboeing, F. and P. Woias, Characterization of different beam shapes for piezoelectric energy harvesting. Journal of micromechanics and microengineering, 2008. 18(10): p. 104013.
[31]. Dietl, J.M. and E. Garcia, Beam shape optimization for power harvesting. Journal of Intelligent Material Systems and Structures, 2010. 21(6): p. 633-646.
[32]. Salmani, H., G. Rahimi, and S. Saraygord Afshari, Optimization of the shaping function of a tapered piezoelectric energy harvester using tabu continuous ant colony system. Journal of Intelligent Material Systems and Structures, 2019. 30(20): p. 3025-3035.
[33]. Liu, W., C. Zhao, A. Badel, F. Formosa, Q. Zhu, and G. Hu, Compact self-powered synchronous energy extraction circuit design with enhanced performance. Smart Materials and Structures, 2018. 27(4): p. 047001.
[34]. Zhao, L., L. Tang, and Y. Yang, Synchronized charge extraction in galloping piezoelectric energy harvesting. Journal of Intelligent Material Systems and Structures, 2016. 27(4): p. 453-468.
[35]. Guyomar, D., A. Badel, E. Lefeuvre, and C. Richard, Toward energy harvesting using active materials and conversion improvement by nonlinear processing. Ieee Transactions on Ultrasonics Ferroelectrics and Frequency Control, 2005. 52(4): p. 584-595.
[36]. Shu, Y.C., I.C. Lien, and W.J. Wu, An improved analysis of the SSHI interface in piezoelectric energy harvesting. Smart Materials and Structures, 2007. 16(6): p. 2253-2264.
[37]. Liang, J. and W. Liao, Impedance modeling and analysis for piezoelectric energy harvesting systems. IEEE/ASME Transactions on Mechatronics, 2012. 17(6): p. 1145-1157.
[38]. Lu, S.H. and F. Boussaid, A Highly Efficient P-SSHI Rectifier for Piezoelectric Energy Harvesting. Ieee Transactions on Power Electronics, 2015. 30(10): p. 5364-5369.
[39]. Liang, J. and W.-H. Liao, Energy flow in piezoelectric energy harvesting systems. Smart Materials and Structures, 2010. 20(1): p. 015005.